

Speculative Decoding Scaling Laws (SDSL): Throughput Optimization Made Simple

Amirhossein Bozorgkhoo* and Igor Molybog†

Abstract

Speculative decoding is a technique that uses multiple language models to accelerate inference. Previous works have used an experimental approach to optimize the throughput of the inference pipeline, which involves LLM training and can be costly. This study of speculative decoding proposes a theory that analytically connects the key hyperparameters of pre-trained LLMs to the throughput efficiency of a downstream SD-based inference system. The theory allows the prediction of throughput-optimal hyperparameters for the components of an inference system before their pre-training.

1 Introduction

Speculative decoding is an effective technique to accelerate Large Language Model (LLM) inference (Chen et al., 2023). It uses a smaller draft model to sequentially generate multiple candidate tokens, which the target model verifies in parallel. Speculative decoding increases throughput while maintaining accuracy. However, the success of this approach is *highly dependent on the choice of the draft model*—an ill-suited draft model can introduce latency bottlenecks, reducing or negating the speedup benefits of speculative decoding. Current methods for selecting an appropriate draft model rely on empirical search and benchmarking across multiple architectures, requiring extensive computational resources and research efforts (Chen et al., 2023; Yan et al., 2024). An overview of the most related literature is provided in Appendix A.

We propose an *analytical framework (scaling law)* for deriving the optimal draft model size ahead of training, assuming it will be trained on a similar dataset to the one used for the target model. This framework is designed to systematically balance draft model inference latency and its accuracy in language modeling tasks.

The main contributions of the paper are:

- We establish a simple analytical relationship of the form

$$\alpha = ax + by + c$$

between draft model perplexity x , target model perplexity y , and their "alignment" α (the expected token acceptance).

- Assuming that both draft and target models are pre-trained from scratch, we derive a numerical relationship of the form

$$N_{\text{opt}} = M_0 + \mu M$$

between the size of the target model M and the optimal draft model N_{opt} . We find that the draft model should be approximately two orders of magnitude (200x) smaller than the target model, and this relationship remains robust across different model families.

- Assuming both models are trained on a comparable scale (on the order of a trillion tokens), the impact of dataset size on throughput remains mild.

We establish a broader Speculative Decoding Scaling Law (SDSL) framework. This framework allows practitioners to adapt the pre-training scaling laws—those connecting perplexity to model size or training dataset properties—for a principled selection of draft models without the need for an additional exhaustive empirical search. The models trained for establishing the pre-training scaling laws can be reused to study the SDSL coefficients a and b for a specific model family. Following our protocol, one can obtain particular values of M_0 and μ without conducting additional experiments and decide on the draft model architecture, given a specific target model size they already have in

*Independent Researcher

†University of Hawai'i at Manoa, Honolulu, HI, USA.

mind. Our framework is developed for throughput measured in token/FLOP, but we validate this further with measuring token/sec and compare with token/FLOP results.

2 Background

2.1 Speculative Decoding

Speculative Decoding utilizes a dual-model architecture to enhance the throughput of token generation in natural language generation tasks. Let M_p denote the **target** language model we would like to use for inference. It outputs the probability distribution over the vocabulary of tokens $p(x_t|x_{<t})$ for a given prefix $x_{<t}$. In contrast, the **draft** language model M_q is a smaller and more compute-efficient language model that could be used for the same task of probability estimation represented by $q(x_t|x_{<t})$ (Leviathan et al., 2023).

The core strategy of Speculative Decoding involves several key steps:

1. Use the efficient model M_q to generate $\gamma \in \mathbb{Z}^+$ completions.
2. Evaluate all generated completions in parallel using the target model M_p . Accept or reject tokens based on a threshold rule.
3. Sample an additional token from an adjusted distribution if the first one is rejected, or add an additional token if all completions are accepted.

For the cost of only running M_p once, this approach can potentially generate up to $\gamma + 1$ new tokens—depending on how well M_q approximates M_p . It also ensures that the sampled tokens are drawn exactly according to the target distribution p . The lookahead length γ represents the maximum number of tokens generated by the draft model.

Expected acceptance α In speculative decoding, a token x_t generated from the distribution $q(x_t|x_{<t})$ can be accepted or rejected according to a threshold rule on $p(x_t|x_{<t})$. The acceptance rate $\beta_{x_{<t}}$ is defined as the probability of accepting a token x_t sampled from the distribution $q(x_t|x_{<t})$, given a prefix $x_{<t}$. To quantify effectiveness of speculative decoding, the parameter

$$\alpha = \mathbb{E}_{x_{<t}}(\beta_{x_{<t}})$$

is introduced, representing the expected acceptance rate across prefixes. The value of α measures how

well the draft distribution aligns with the target distribution (Leviathan et al., 2023). The practical method we use for estimating α is provided in Appendix B.

Throughput Enhancement in Speculative Decoding

Leviathan et al. (2023) analyze how their speculative decoding algorithm enhances inference efficiency by reducing wall-clock time. They demonstrate that, under the assumption of independent and identically distributed (i.i.d.) inputs, their method decreases the number of calls to the target model, M_p , by a factor of $\frac{1-\alpha^{\gamma+1}}{1-\alpha}$. This reduction is contingent on having sufficient computational resources to support increased concurrency, allowing for $\gamma + 1$ concurrent evaluations of M_p without extending wall-clock time.

To quantify wall-clock time improvement, they introduce a cost coefficient c , which represents the ratio of the time taken for a single run of the approximation model M_q relative to that of M_p . In their experiments, c is consistently less than 0.05, indicating that M_q is significantly smaller and faster than M_p . The authors derive a theorem stating that the expected improvement factor in total wall-clock time using their algorithm is given by

$$\frac{\text{Spec dec Throughput}}{M_p \text{ Throughput}} = \frac{1 - \alpha^{\gamma+1}}{(1 - \alpha)(\gamma c + 1)}. \quad (1)$$

Furthermore, they establish a corollary indicating that if $\alpha > c$, there exists a value of γ that leads to an improvement in wall-clock time, with a minimum improvement factor of at least $\frac{1+\alpha}{1+c}$. This analysis underscores the potential for significant throughput improvements in practical applications of their speculative decoding approach, particularly when computational resources are adequately provisioned.

However, the connection between c and α observed for modern language models remains unexplored, which is the gap our work is aiming to fill.

2.2 Scaling Laws for Pre-training

Scaling laws were previously developed to inform decision-making during the design stage of large-scale training experiments. The scaling laws for pre-training of large language models analytically relate the key metrics of the trained model performance, such as cross-entropy loss L , to the key hyperparameters of the training routine, such as the number of model parameters N and the number of

training tokens D . A common way to capture the dependency is in the form suggested by Hoffmann et al. (2022)

$$L(N, D) = \ln x(N, D) = E + \frac{A}{N^\nu} + \frac{B}{D^\delta}, \quad (2)$$

The constants E , A , B , ν , and δ are parameters that capture the irreducible loss and the diminishing returns on loss reduction as model size and training data increase. Specifically, A/N^ν models the effect of increasing model size on loss, while B/D^δ accounts for the impact of additional training tokens.

Similarly, the presented work aims to develop a scaling law of an inference system to inform decision-making during the design stage of an AI service.

3 Methodology

3.1 FLOPs of a Speculative Decoding iteration

We first compute throughput in terms of tokens per inference FLOP, which allows us to abstract away from any specific hardware configuration. This formulation is motivated by the strong correlation between inference wall-clock time and the computational workload of the inference process. We then validate this approach by measuring wall-clock latency across draft–target pairs. We find this methodology to be more objective, as it naturally adapts to rapid advances in hardware performance.

As shown by Kaplan et al. (2020), the total number of floating point operations (FLOPs) for a transformer model during a forward pass with a small context length can be efficiently approximated by $2N$, where N is the number of parameters (size) of the model. Here and further in the paper, the size of the target model is denoted as M , while N is reserved for the size of the draft model. During each iteration, the draft model generates γ speculative guesses, requiring $2N\gamma$ FLOPs for a forward pass through the draft model. Additionally, for each guess generated, the target model evaluates these guesses in parallel, incurring another $2M$ FLOPs. Therefore, the total computational cost of a single speculative decoding iteration is $2(M + \gamma \cdot N)$.

3.2 Modeling Throughput

Yan et al. (2025) presented a formula for the throughput of a speculative decoding system expressed in tokens per second. We adapt their approach to express throughput in tokens per FLOP.

We accept $c = \frac{N}{M}$ and use (1) to establish that the throughput of speculative decoding is proportional to

$$\mathcal{T} = \frac{1 - \alpha^{\gamma+1}}{2(M + \gamma \cdot N)(1 - \alpha)}, \quad (3)$$

with an architecture-defined proportionality coefficient.

The value of lookahead length γ can be set arbitrarily, complicating the analysis of optimal throughput. To abstract this hyperparameter out, we assume the value of γ to be optimally chosen. In Appendix C, we show that the throughput under optimal γ is captured through

$$\mathcal{T} = \frac{-\log(\alpha)}{2N(-1 + \alpha)W\left(-\frac{\alpha^{M/N-1}}{e}\right)} \quad (4)$$

where W denotes the Lambert W function. The dependency of α on the other hyperparameters is the focus of the experimental part of our work.

4 Experiments

We aim to derive an analytical expression that relates the throughput of a speculative decoding system to the training hyperparameters of the component models, primarily the sizes of the draft (N) and target (M) models, but also the amount of data (D) they are trained on. To achieve this, we study the dependency of α on the perplexity characteristics of the target and draft models. After that, we use the pre-training scaling laws relating the perplexity metrics to the model hyperparameters and combine them with (4).

We evaluate our framework on a diverse set of LLMs, spanning multiple model families, including LLaMA 3 (Grattafiori et al., 2024), LLaMA 3.1 (AI, 2024), OPT (Zhang et al., 2022), Qwen 1.5 (Bai et al., 2023), Qwen 2.5 (Team, 2024), and an open-source model released by ByteDance Seed (Team, 2025).

4.1 Estimating α values

Setup. We utilize the Microsoft DeepSpeed library (Microsoft, 2023) to implement speculative decoding, following the methodology discussed in Appendix B.

The target and draft model pairs used in our experiments are indicated in Tables 1 and 2. We evaluate the perplexity of these models on the HellaSwag (Zellers et al., 2019) dataset, which consists of commonsense reasoning tasks requiring models to complete sentences based on provided contexts.

	Draft Model	OPT-125M	OPT-350M	OPT-1.3B	OPT-2.7B
Target Model	Perplexity	29.79318619	25.32799339	19.36876869	17.36415863
OPT-13B	15.58453751	0.5959 \pm 0.0018	0.6281 \pm 0.0017	0.6694 \pm 0.0016	0.6793 \pm 0.0016
OPT-30B	15.30226898	0.6779 \pm 0.0017	0.6984 \pm 0.0016	0.7325 \pm 0.0015	0.7447 \pm 0.0015
OPT-66B	14.58085632	0.7118 \pm 0.0016	0.7342 \pm 0.0015	0.7659 \pm 0.0014	0.7847 \pm 0.0014
Qwen1.5-14B	11.7312355	0.599 \pm 0.0013	0.6178 \pm 0.0012	0.6569 \pm 0.0012	0.6708 \pm 0.0012
Qwen1.5-32B	10.41608143	0.5842 \pm 0.0013	0.6086 \pm 0.0013	0.6458 \pm 0.0012	0.6617 \pm 0.0012
Qwen1.5-72B	10.33209324	0.5929 \pm 0.0013	0.6177 \pm 0.0013	0.6511 \pm 0.0012	0.6658 \pm 0.0012
Qwen1.5-110B	10.07259178	0.5206 \pm 0.0013	0.5461 \pm 0.0013	0.5816 \pm 0.0013	0.5981 \pm 0.0013
Qwen2.5-14B	10.29567051	0.5998 \pm 0.0021	0.6184 \pm 0.002	0.653 \pm 0.0019	0.6651 \pm 0.0019
Qwen2.5-32B	9.549574852	0.5755 \pm 0.0019	0.5954 \pm 0.0018	0.632 \pm 0.0017	0.6495 \pm 0.0017
Qwen2.5-72B	10.11350441	0.5702 \pm 0.0019	0.5917 \pm 0.0019	0.6245 \pm 0.0018	0.6443 \pm 0.0018
LLaMa3-70B	11.00730228	0.6027 \pm 0.0014	0.6282 \pm 0.0013	0.6605 \pm 0.0013	0.6744 \pm 0.0013
LLaMa3.1-70B	11.07195759	0.6057 \pm 0.0018	0.6246 \pm 0.0018	0.6647 \pm 0.0017	0.6738 \pm 0.0017
Seed-OSS-36B	9.997225761	0.5347 \pm 0.0022	0.557 \pm 0.0022	0.5861 \pm 0.0021	0.6033 \pm 0.0021

Table 1: Estimated α values along with their associated 95% confidence intervals (associated with stochasticity in evaluation and not training) and measured perplexity for selected pairs of all target models and OPT draft models.

Target Model	Draft Model	Qwen2.5-0.5B	Qwen2.5-1.5B	Qwen2.5-3B	Qwen1.5-0.5B	Qwen1.5-1.8B	Qwen1.5-4B
	Perplexity	17.91464424	13.69491291	12.5883894	18.37218094	14.10007191	13.90737915
OPT-13B	15.58453751	0.6516 \pm 0.0017	0.6678 \pm 0.0017	0.6725 \pm 0.0016	0.649 \pm 0.0017	0.6672 \pm 0.0017	0.6716 \pm 0.0017
OPT-30B	15.30226898	0.7282 \pm 0.0016	0.7414 \pm 0.0015	0.749 \pm 0.0015	0.7241 \pm 0.0016	0.7372 \pm 0.0015	0.7483 \pm 0.0015
OPT-66B	14.58085632	0.7678 \pm 0.0014	0.7881 \pm 0.0013	0.7882 \pm 0.0013	0.7634 \pm 0.0013	0.7808 \pm 0.0014	0.7875 \pm 0.0014
Qwen1.5-14B	11.7312355	0.6898 \pm 0.0011	0.7244 \pm 0.0011	0.7323 \pm 0.0011	0.6838 \pm 0.0011	0.7131 \pm 0.0011	0.7343 \pm 0.0011
Qwen1.5-32B	10.41608143	0.6698 \pm 0.0012	0.7069 \pm 0.0011	0.7152 \pm 0.0011	0.6585 \pm 0.0012	0.6873 \pm 0.0012	0.7084 \pm 0.0011
Qwen1.5-72B	10.33209324	0.6685 \pm 0.0012	0.7065 \pm 0.0011	0.7156 \pm 0.0011	0.6607 \pm 0.0012	0.6848 \pm 0.0012	0.7079 \pm 0.0011
Qwen1.5-110B	10.07259178	0.6064 \pm 0.0012	0.6399 \pm 0.0012	0.6503 \pm 0.0012	0.5907 \pm 0.0013	0.6215 \pm 0.0012	0.6401 \pm 0.0012
Qwen2.5-14B	10.29567051	0.6783 \pm 0.0013	0.7109 \pm 0.0012	0.7202 \pm 0.0012	0.6742 \pm 0.0019	0.6878 \pm 0.0018	0.7089 \pm 0.0017
Qwen2.5-32B	10.11350441	0.6698 \pm 0.0012	0.7111 \pm 0.0011	0.722 \pm 0.0011	0.6651 \pm 0.0017	0.6863 \pm 0.0016	0.7062 \pm 0.0016
Qwen2.5-72B	9.549574852	0.6663 \pm 0.0012	0.7079 \pm 0.0011	0.7139 \pm 0.0011	0.6525 \pm 0.0018	0.6757 \pm 0.0017	0.7006 \pm 0.0016
LLaMa3-70B	11.00730228	0.6959 \pm 0.0012	0.7367 \pm 0.0011	0.7408 \pm 0.0011	0.6815 \pm 0.0017	0.705 \pm 0.0017	0.7283 \pm 0.0016
LLaMa3.1-70B	11.07195759	0.6699 \pm 0.0017	0.7035 \pm 0.0016	0.7149 \pm 0.0016	0.6584 \pm 0.0017	0.6816 \pm 0.0017	0.6998 \pm 0.0016
Seed-OSS-36B	9.997225761	0.5998 \pm 0.0021	0.6313 \pm 0.002	0.6422 \pm 0.002	0.5855 \pm 0.0021	0.6079 \pm 0.0021	0.6264 \pm 0.002

Table 2: Estimated α values along with their associated 95% confidence intervals (associated with stochasticity in evaluation and not training) and measured perplexity for selected pairs of all target models and Qwen draft models.

We use an open-ended generation strategy, enabling models to produce full responses rather than single-letter answers, better reflecting real-world usage and commonsense reasoning capabilities.

Implementation Framework. In our setup, we generated human-readable ground-truth text from the target, then re-tokenized this output using the draft model’s tokenizer. This ensured compatibility and allowed reliable cross-family evaluation. This consistent process was applied across all target–draft pairs for Tables 1 and 2.

Perplexity Calculation. We used Qwen 2.5, Qwen 1.5 and OPT draft models, computing perplexity on HellaSwag with a max sequence length of 2048. Longer documents were truncated accordingly.

Results. The empirical estimations of the α values and perplexity across various pairs of target and

draft models are collected in Tables 1 and 2. Across all target models, the larger draft models with lower values of perplexity correspond to higher estimated α values. The dependency of α on the target model size is less pronounced, as evident from the experiments conducted for various target models.

4.2 Regressing α on perplexity of draft and target models

To analyze the relationship between draft model perplexity, target model perplexity and estimated α values, we fitted an affine plane as a scaling law to the data presented in Tables 1 and 2 :

$$\alpha = Ax + By + C \quad (5)$$

Where x is perplexity of the draft model and y is the perplexity of the target model. The estimated values of its parameters, R-squared and Mean Squared Error (MSE) are collected in Table 3 . The fitted

relationship is illustrated in Figure 1.

Discussion. The dependence of the scaling parameter α on draft model perplexity and target model perplexity is analyzed separately in Appendix D and Appendix E. Our results show a strong and systematic dependence of α on draft model perplexity, characterized by a consistent monotonic increase in α as draft model perplexity decreases across all target models and fitted functional forms. In contrast, the dependence of α on target model perplexity is comparatively weak and does not exhibit a robust or consistent trend when the draft model is held fixed.

Despite this asymmetry, we retain both draft and target model perplexities as explanatory variables in the affine scaling law of Equation (5). While draft model perplexity constitutes the dominant factor governing variations in α , incorporating target model perplexity ensures that the scaling law accounts for residual target-dependent effects and remains applicable across a broad range of model families and quality regimes. Equation (5) captures

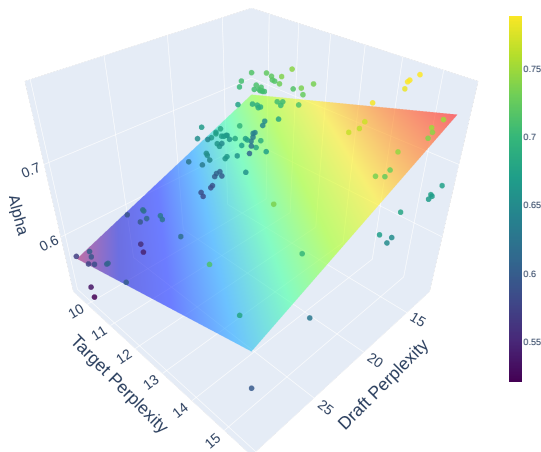


Figure 1: Visualization of the fitted affine plane relating the estimated scaling parameter α to draft model perplexity (x) and target model perplexity (y). Scatter points represent empirical (x, y, α) observations from Tables 1 and 2, while the surface corresponds to the least-squares fit of Equation 5.

the dependency of α on the perplexity of the draft model x and perplexity of the target model y . Incorporating this into (4) results in the following formula for throughput:

$$\mathcal{T} = \frac{-\log(Ax + By + C)}{2N(Ax + By + C - 1)W\left(-\frac{(Ax + By + C)^{\frac{M}{N}-1}}{e}\right)} \quad (6)$$

4.3 Throughput vs size of the draft and target models

Working with a specific pre-training dataset and a specific training recipe, one can fit setup-specific scaling law parameters A , B and C , since they depend on the properties of the training setup.

To connect throughput to the training hyperparameters of the component models, we use the scaling law (2) that relates the perplexity of a trained model to its size and the size of its training dataset. We first utilize the parameters suggested by Besiroglu et al. (2024) :

$$x = e^{1.8172 + \frac{482.01}{N-0.3478} + \frac{2085.43}{D-0.3658}} \quad (7)$$

$$y = e^{1.8172 + \frac{482.01}{M-0.3478} + \frac{2085.43}{D'-0.3658}} \quad (8)$$

where D and D' are the number of training tokens used in the draft and target models, respectively. Similarly to A , B and C , the training setup defines the exact parameter values and could be estimated for a specific training dataset at hand. After substituting these expressions into (6), one gets an expression for throughput exclusively through the core parameters of the components of a speculative training system: M , N , and D .

$$\mathcal{T} = \frac{-\log(Ae^{L(N,D)} + Be^{L(M,D')} + C)}{2N(Ae^{L(N,D)} + Be^{L(M,D')} + C - 1)} \cdot \frac{1}{W\left(\frac{(Ae^{L(N,D)} + Be^{L(M,D')} + C)^{M/N-1}}{-e}\right)} \quad (9)$$

Equation (9) captures the dependency of Throughput on the size of the target and draft model along with size of the dataset used to train the target and draft models.

To examine the relationship between throughput and draft model size N , we numerically analyzed Equation (9) using input values from our model families. Through grid search, we estimated the values of N that yield local throughput maxima, denoted as N^* , with results shown in Table 5. We empirically validate this throughput-based prediction by measuring end-to-end inference latency under speculative decoding for an OPT-13B target model, with results reported in Appendix F.

In Figure 2, each curve depicts the predicted throughput as a function of the draft model size N for a fixed target model, with separate panels corresponding to the draft model families. For each target model, the optimal draft size N^* that maximizes throughput is indicated by a star marker placed directly on the curve, while black markers denote the draft model sizes used in our experiments. Across all draft families, throughput initially increases with N , reflecting higher acceptance rates and reduced reliance on the target model.

The observed curvature at the end of the throughput curves is a direct result of the diminishing efficiency of speculative decoding when the draft and target models are similar in size. When $N \approx M$, the computational savings from using a draft model vanish, since both models require nearly the same amount of FLOPs. Consequently, speculative decoding no longer provides a speedup, and throughput decreases instead of increasing. This results in a negative derivative of throughput with respect to N near $N = M$, causing the observed curvature on the right-hand side of the curves.

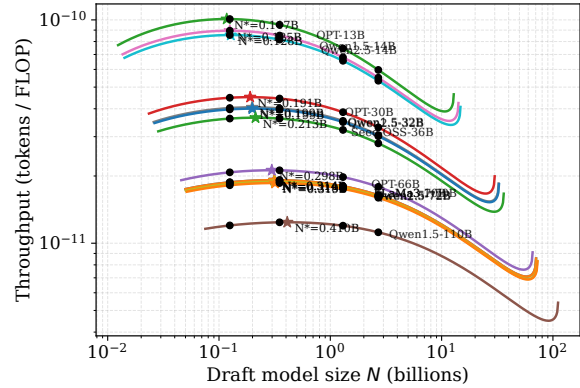
5 Throughput-optimal draft models

This Section is dedicated to the analysis of the draft model size N^* that maximizes the predicted value of throughput presented in (9). We study in more detail how N^* depends on the size of the target model M and the amount of available data for training the draft model D and target model D' .

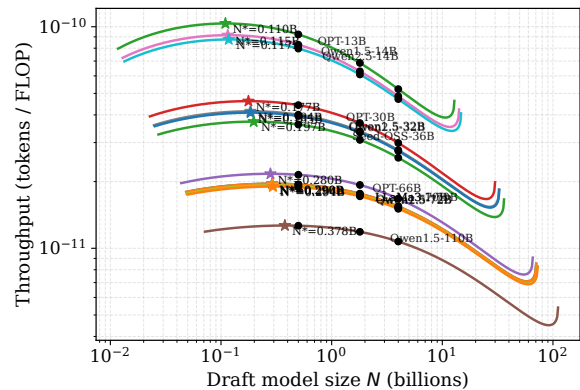
5.1 Motivation and Numerical Approximation Methodology

We aim to derive a simple, reusable rule linking the optimal draft model size N^* to the target model size M and dataset sizes of the draft model D and target model D' . While the ideal approach is to maximize throughput from Equation (9) with respect to N , the equation’s complexity renders analytical optimization intractable.

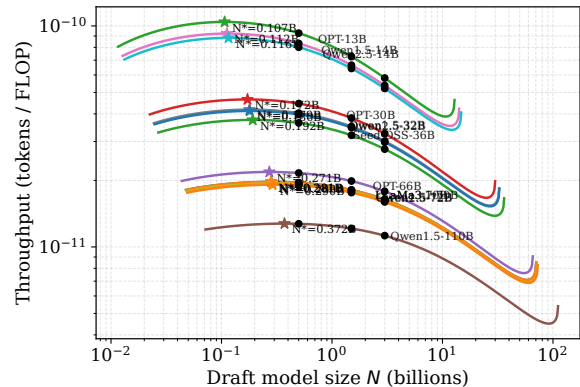
Instead, we study Equation (9) numerically, evaluating throughput over a dense mesh of (N, D, M, D') values. Parameters are sampled from logarithmically spaced ranges (Table 7) to reflect realistic LLM scaling scenarios. For each (D, M, D') , we identified the N value yielding the highest throughput as N^* .



(a) Throughput predicted by (9) for the target models paired with OPT-based draft models.



(b) Throughput predicted by (9) for the target models paired with Qwen1.5-based draft models.



(c) Throughput predicted by (9) for the target models paired with Qwen2.5-based draft models.

Figure 2: Throughput (tokens per FLOP) predicted by Equation (9) as a function of draft model size N (in billions of parameters) for different target models and draft model families based on Table 5. Each curve corresponds to a single target model and is annotated directly on the curve. Black markers indicate the draft model sizes used in experiments, while star markers denote the optimal draft size N^* that maximizes predicted throughput for each target model.

Across a broad range of target model sizes M , draft training dataset sizes D , and target training dataset sizes D' , the dominant trend is a strong and

approximately linear growth of N^* with the target model size. In contrast, variations in the training dataset sizes introduce only mild modulations of this behavior. These trends are illustrated in Figure 5.

5.2 Basic Observation

The numerical analysis of Equation (9) reveals a clear and systematic structure in the dependence of the throughput-optimal draft model size N^* on the properties of the speculative decoding system.

In Figure 5a, the optimal draft size increases monotonically with the target model size M , and this trend is consistent across all examined values of the draft training dataset size D . This behavior indicates that the dominant factor governing the magnitude of the optimal draft model size is the target model size itself. The upward trend in N^* reflects the need for larger draft models as the target grows, while the downward trend in N^*/M indicates that this growth is approximately linear, with diminishing finite-size corrections. In contrast, Figure 5c shows that varying the draft training dataset size D at fixed M leads to only modest changes in N^* , suggesting that the influence of D is secondary.

To isolate these secondary effects, Figure 5b and Figure 5d present the normalized quantity N^*/M . Normalization largely collapses the curves across different values of D , indicating that the primary scaling of the optimal draft size is approximately linear in the target model size. Residual variation in N^*/M across both M and D is mild and systematic, reflecting sublinear corrections rather than a change in the dominant scaling behavior.

Finally, Figures 5e and 5f examine the sensitivity of the optimal draft size to the target training dataset size D' . Both the raw and normalized plots show that variations in D' have a negligible effect on N^* relative to the effects of M and D , indicating that target-side training data introduces only minor second-order corrections to the draft model sizing rule.

5.3 Analytical Approximation of the Throughput-Optimal Draft Size

Motivated by the observed near-collapse of the normalized quantity N^*/M in Section 5.2, we seek an analytical approximation that captures the leading scaling behavior while remaining interpretable and reusable. In particular, the numerical results suggest that N^*/M approaches a constant for large M ,

with finite-size corrections that decay sub-linearly. This motivates the following scaling ansatz:

$$\frac{N^*}{M} = \mu + \frac{M_0}{M} + \gamma \log D + \gamma' \log D', \quad (10)$$

where μ represents the asymptotic draft-to-target size ratio, M_0 captures finite-size corrections, and the coefficients γ and γ' quantify residual dependence on the draft and target training dataset sizes, respectively.

We estimate the parameters in Equation (10) by fitting to the numerically computed optima $N^*(M, D, D')$ obtained from exhaustive search over the draft size N for each configuration of (M, D, D') . Each regression observation corresponds to one point in the Cartesian product of the logarithmically spaced grids in M , D , and D' . The draft-size grid over N is used solely for the inner numerical optimization and does not contribute additional regression degrees of freedom. Ordinary least squares with heteroskedasticity-robust (HC3) standard errors is used to account for scale-dependent variance across model sizes.

The fitted parameters, reported in Table 8, confirm that the leading-order behavior of the throughput-optimal draft size is linear in the target model size. The asymptotic ratio μ is tightly constrained, indicating that for sufficiently large target models the optimal draft is approximately constant in relative size. The finite-size term M_0/M explains the systematic decrease of N^*/M with increasing M observed in the numerical results.

Dataset-size effects enter only as small corrections. The coefficient γ is negative and statistically significant, indicating that increasing the amount of draft training data slightly reduces the optimal relative draft size, while the coefficient γ' associated with the target training dataset is statistically indistinguishable from zero. This confirms that target-side data availability has a negligible impact on draft sizing compared to the dominant dependence on M .

5.4 Summary

We analyzed how the throughput-optimal draft model size N^* depends on the target model size M and the training dataset sizes (D, D') . The numerical results show that, across a wide range of configurations, the dominant factor governing the optimal draft size is the target model size itself, while dataset-related effects introduce only secondary corrections. Motivated by this observation,

we derived a simplified leading-order scaling law that models N^* solely as a function of M .

Using the full set of numerically computed optima across all combinations of (M, D, D_t) , we performed a pooled linear regression to obtain a robust analytical approximation of the form

$$N^*(M) = \mu M + M_0. \quad (11)$$

The fitted coefficients, along with their margins of error and confidence intervals, are reported in Table 9. This affine relation implies that the ratio N^*/M varies with target model size due to finite-size effects captured by the offset term M_0 .

For smaller target models, the additive constant M_0 inflates the relative draft size, whereas its influence diminishes as M increases. In the large- M regime, the ratio N^*/M converges to the asymptotic value $\mu \approx 2.7 \times 10^{-3}$, indicating that the throughput-optimal draft model is approximately 200 \times smaller than the target. This convergence explains the systematic decrease of N^*/M observed in the numerical results and the near-collapse of normalized curves at large model sizes.

This asymptotic prediction provides a useful theoretical benchmark for speculative decoding. Empirical studies commonly explore draft-to-target size ratios spanning more than two orders of magnitude, with throughput-optimal configurations typically corresponding to draft models that are tens to hundreds of times smaller than the target. The scaling law derived here falls squarely within this empirically relevant regime, reinforcing its practical utility as a guideline for selecting draft model sizes in large-scale speculative decoding systems.

6 Conclusion

Speculative decoding accelerates large language model (LLM) inference by delegating token proposal to a lightweight draft model while relying on a larger target model for parallel verification. The effectiveness of this approach, however, is highly sensitive to the choice of the draft model, and suboptimal selections can significantly diminish throughput gains. Prior work has largely relied on empirical benchmarking to identify suitable draft models, resulting in increased deployment complexity and computational overhead.

In this work, we introduced **Speculative Decoding Scaling Laws (SDSL)**, an analytical framework that connects pre-training scaling laws to the

throughput efficiency of speculative decoding systems. We showed that the expected token acceptance rate can be accurately modeled as an affine function of draft and target model perplexities, with draft model quality emerging as the dominant factor. By integrating this relationship with established pre-training scaling laws, we derived a principled, closed-form characterization of speculative decoding throughput in terms of model size and training data.

Our analysis reveals a robust and generalizable result: across model families, training regimes, and dataset scales, the throughput-optimal draft model size scales approximately linearly with the target model size, while dataset-related effects introduce only mild second-order corrections. In the large-model regime, this relationship converges to a constant draft-to-target size ratio on the order of 10^{-3} , indicating that the optimal draft model is approximately 200 \times smaller than the target. This prediction aligns closely with empirical observations across modern LLM families and provides a theoretical explanation for the regimes in which speculative decoding is most effective.

While our formulation is derived in terms of tokens per FLOP, we further validated its practical relevance through wall-clock latency measurements, demonstrating consistency across evaluation metrics.

7 Limitations

Our framework assumes that both draft and target models are trained on comparable data distributions and with similar training recipes. Deviations from this assumption—such as heavy domain specialization, substantial architectural asymmetry, or aggressive post-training alignment—may affect the quantitative accuracy of the scaling coefficients, even if the qualitative trends remain valid.

In addition, our analysis focuses exclusively on autoregressive text-only language models. We do not consider alternative architectures such as encoder–decoder models, mixture-of-experts systems, or multi-modal models incorporating visual or audio inputs. Extending SDSL to these settings may require additional modeling assumptions and empirical validation.

Acknowledgements

This work was supported by the National Science Foundation NRT-AI 2244574.

References

- Meta AI. 2024. Introducing Llama 3.1: Our most capable models to date. <https://ai.meta.com/blog/meta-llama-3-1/>.
- Jinze Bai, Shuai Bai, Yunfei Chu, Zeyu Cui, Kai Dang, Xiaodong Deng, Yang Fan, Wenbin Ge, Yu Han, Fei Huang, Binyuan Hui, Luo Ji, Mei Li, Junyang Lin, Runji Lin, Dayiheng Liu, Gao Liu, Chengqiang Lu, Keming Lu, Jianxin Ma, Rui Men, Xingzhang Ren, Xuancheng Ren, Chuanqi Tan, Sinan Tan, Jianhong Tu, Peng Wang, Shijie Wang, Wei Wang, Shengguang Wu, Benfeng Xu, Jin Xu, An Yang, Hao Yang, Jian Yang, Shusheng Yang, Yang Yao, Bowen Yu, Hongyi Yuan, Zheng Yuan, Jianwei Zhang, Xingxuan Zhang, Yichang Zhang, Zhenru Zhang, Chang Zhou, Jingren Zhou, Xiaohuan Zhou, and Tianhang Zhu. 2023. Qwen technical report. *arXiv preprint arXiv:2309.16609*.
- Tamay Besiroglu, Ege Erdil, Matthew Barnett, and Josh You. 2024. [Chinchilla scaling: A replication attempt](#). *Preprint*, arXiv:2404.10102.
- Charlie Chen, Sebastian Borgeaud, Geoffrey Irving, Jean-Baptiste Lespiau, Laurent Sifre, and John Jumper. 2023. Accelerating large language model decoding with speculative sampling. *arXiv preprint arXiv:2302.01318*.
- Jian Chen, Vashisth Tiwari, Ranajoy Sadhukhan, Zhuoming Chen, Jinyuan Shi, Ian En-Hsu Yen, and Beidi Chen. 2024. Magicdec: Breaking the latency-throughput tradeoff for long context generation with speculative decoding. *arXiv preprint arXiv:2408.11049*.
- Aaron Grattafiori, Abhimanyu Dubey, Abhinav Jauhri, Abhinav Pandey, Abhishek Kadian, Ahmad Al-Dahle, Aiesha Letman, Akhil Mathur, Alan Schelten, Alex Vaughan, Amy Yang, Angela Fan, Anirudh Goyal, Anthony Hartshorn, Aobo Yang, Archi Mitra, Archie Sravankumar, Artem Korenev, Arthur Hinsvark, Arun Rao, Aston Zhang, Aurelien Rodriguez, Austen Gregerson, Ava Spataru, Baptiste Roziere, Bethany Biron, Binh Tang, Bobbie Chern, Charlotte Caucheteux, Chaya Nayak, Chloe Bi, Chris Marra, Chris McConnell, Christian Keller, Christophe Touret, Chunyang Wu, Corinne Wong, Cristian Canton Ferrer, Cyrus Nikolaidis, Damien Allonsius, Daniel Song, Danielle Pintz, Danny Livshits, Danny Wyatt, David Esiobu, Dhruv Choudhary, Dhruv Mahajan, Diego Garcia-Olano, Diego Perino, Dieuwke Hupkes, Egor Lakomkin, Ehab AlBadawy, Elina Lobanova, Emily Dinan, Eric Michael Smith, Filip Radenovic, Francisco Guzmán, Frank Zhang, Gabriel Synnaeve, Gabrielle Lee, Georgia Lewis Anderson, Govind Thattai, Graeme Nail, Gregoire Mialon, Guan Pang, Guillem Cucurell, Hailey Nguyen, Hannah Korevaar, Hu Xu, Hugo Touvron, Iliyan Zarov, Imanol Arrieta Ibarra, Isabel Kloumann, Ishan Misra, Ivan Evtimov, Jack Zhang, Jade Copet, Jaewon Lee, Jan Geffert, Jana Vranes, Jason Park, Jay Mahadeokar, Jeet Shah, Jelmer van der Linde, Jennifer Billock, Jenny Hong, Jenya Lee, Jeremy Fu, Jianfeng Chi, Jianyu Huang, Jiawen Liu, Jie Wang, Jiecao Yu, Joanna Bitton, Joe Spisak, Jongsoo Park, Joseph Rocca, Joshua Johnstun, Joshua Saxe, Junteng Jia, Kalyan Vasuden Alwala, Karthik Prasad, Kartikeya Upasani, Kate Plawiak, Ke Li, Kenneth Heafield, Kevin Stone, Khalid El-Arini, Krithika Iyer, Kshitiz Malik, Kuenley Chiu, Kunal Bhalla, Kushal Lakhotia, Lauren Rantala-Yearly, Laurens van der Maaten, Lawrence Chen, Liang Tan, Liz Jenkins, Louis Martin, Lovish Madaan, Lubo Malo, Lukas Blecher, Lukas Landzaat, Luke de Oliveira, Madeline Muzzi, Mahesh Pasupuleti, Mannat Singh, Manohar Paluri, Marcin Kardas, Maria Tsimpoukelli, Mathew Oldham, Mathieu Rita, Maya Pavlova, Melanie Kam-badur, Mike Lewis, Min Si, Mitesh Kumar Singh, Mona Hassan, Naman Goyal, Narjes Torabi, Nikolay Bashlykov, Nikolay Bogoychev, Niladri Chatterji, Ning Zhang, Olivier Duchenne, Onur Çelebi, Patrick Alrassy, Pengchuan Zhang, Pengwei Li, Petar Vasic, Peter Weng, Prajjwal Bhargava, Pratik Dubal, Praveen Krishnan, Punit Singh Koura, Puxin Xu, Qing He, Qingxiao Dong, Ragavan Srinivasan, Raj Ganapathy, Ramon Calderer, Ricardo Silveira Cabral, Robert Stojnic, Roberta Raileanu, Rohan Maheswari, Rohit Girdhar, Rohit Patel, Romain Sauvestre, Ronnie Polidoro, Roshan Sumbaly, Ross Taylor, Ruan Silva, Rui Hou, Rui Wang, Saghar Hosseini, Sahana Chennabasappa, Sanjay Singh, Sean Bell, Seohyun Sonia Kim, Sergey Edunov, Shaoliang Nie, Sharan Narang, Sharath Rapparthi, Sheng Shen, Shengye Wan, Shruti Bhosale, Shun Zhang, Simon Vandenhende, Soumya Batra, Spencer Whitman, Sten Sootla, Stephane Collet, Suchin Gururangan, Sydney Borodinsky, Tamar Herman, Tara Fowler, Tarek Sheasha, Thomas Georgiou, Thomas Scialom, and Tobias Speckbacher. 2024. [The Llama 3 Herd of Models](#). *arXiv e-prints*, arXiv:2407.21783.
- Jiatao Gu, Yuyang Wang, Yizhe Zhang, Qihang Zhang, Dinghuai Zhang, Navdeep Jaitly, Josh Susskind, and Shuangfei Zhai. 2025. [Dart: Denoising autoregressive transformer for scalable text-to-image generation](#). *Preprint*, arXiv:2410.08159.
- Jordan Hoffmann, Sebastian Borgeaud, Arthur Mensch, Elena Buchatskaya, Trevor Cai, Eliza Rutherford, Diego de Las Casas, Lisa Anne Hendricks, Johannes Welbl, Aidan Clark, Tom Hennigan, Eric Noland, Katie Millican, George van den Driessche, Bogdan Damoc, Aurelia Guy, Simon Osindero, Karen Simonyan, Erich Elsen, Jack W. Rae, Oriol Vinyals, and Laurent Sifre. 2022. [Training compute-optimal large language models](#). *Preprint*, arXiv:2203.15556.
- Jared Kaplan, Sam McCandlish, Tom Henighan, Tom B. Brown, Benjamin Chess, Rewon Child, Scott Gray, Alec Radford, Jeffrey Wu, and Dario Amodei. 2020. [Scaling laws for neural language models](#). *Preprint*, arXiv:2001.08361.
- Yaniv Leviathan, Matan Kalman, and Yossi Matias. 2023. [Fast inference from transformers via speculative decoding](#). *Preprint*, arXiv:2211.17192.

- Xiaoxuan Liu, Lanxiang Hu, Peter Bailis, Ion Stoica, Zhijie Deng, Alvin Cheung, and Hao Zhang. 2023. Online speculative decoding. *arXiv preprint arXiv:2310.07177*.
- Microsoft. 2023. Deepspeed. <https://github.com/microsoft/deepspeed>. Accessed: January 26, 2024.
- Hanshi Sun, Zhuoming Chen, Xinyu Yang, Yuandong Tian, and Beidi Chen. 2024a. Triforce: Lossless acceleration of long sequence generation with hierarchical speculative decoding. *arXiv preprint arXiv:2404.11912*.
- Ziteng Sun, Ananda Theertha Suresh, Jae Hun Ro, Ahmad Beirami, Himanshu Jain, and Felix Yu. 2024b. Spectr: Fast speculative decoding via optimal transport. *Preprint*, arXiv:2310.15141.
- ByteDance Seed Team. 2025. Seed-oss open-source models. <https://github.com/ByteDance-Seed/seed-oss>.
- Qwen Team. 2024. Qwen2.5: A party of foundation models.
- Heming Xia, Tao Ge, Peiyi Wang, Si-Qing Chen, Furu Wei, and Zhifang Sui. 2023. Speculative decoding: Exploiting speculative execution for accelerating seq2seq generation. In *Findings of the Association for Computational Linguistics: EMNLP 2023*, pages 3909–3925.
- Minghao Yan, Saurabh Agarwal, and Shivaram Venkataraman. 2024. Decoding speculative decoding. *Preprint*, arXiv:2402.01528.
- Minghao Yan, Saurabh Agarwal, and Shivaram Venkataraman. 2025. Decoding speculative decoding. *Preprint*, arXiv:2402.01528.
- Sen Yang, Shujian Huang, Xinyu Dai, and Jiajun Chen. 2024. Multi-candidate speculative decoding. *arXiv preprint arXiv:2401.06706*.
- Rowan Zellers, Ari Holtzman, Yonatan Bisk, Ali Farhadi, and Yejin Choi. 2019. Hellaswag: Can a machine really finish your sentence? *arXiv preprint arXiv:1905.07830*.
- Jun Zhang, Jue Wang, Huan Li, Lidan Shou, Ke Chen, Gang Chen, and Sharad Mehrotra. 2023. Draft & verify: Lossless large language model acceleration via self-speculative decoding. *arXiv preprint arXiv:2309.08168*.
- Susan Zhang, Stephen Roller, Naman Goyal, Mikel Artetxe, Moya Chen, Shuohui Chen, Christopher Dewan, Mona Diab, Xian Li, Xi Victoria Lin, et al. 2022. Opt: Open pre-trained transformer language models. *arXiv preprint arXiv:2205.01068*.
- Yongchao Zhou, Kaifeng Lyu, Ankit Singh Rawat, Aditya Krishna Menon, Afshin Rostamizadeh, Sanjiv Kumar, Jean-François Kagy, and Rishabh Agarwal. 2024. Distillspec: Improving speculative decoding via knowledge distillation. In *The Twelfth International Conference on Learning Representations*.

A Related Works

Optimizing draft model design has been a key area of research for improving speculative decoding efficiency. Yan et al. (2025) conducted a comprehensive benchmarking study to investigate the factors that influence throughput improvements in speculative decoding. They identified **draft model latency** as the primary bottleneck, highlighting that deeper models with the same parameter count exhibit higher latency. Furthermore, they observed that **accuracy on language modeling tasks** does not strongly correlate with speculative decoding performance, suggesting that choosing a draft model based solely on accuracy may be sub-optimal for maximizing throughput. To address these issues, the authors propose redesigning draft models by adjusting their depth-to-width ratio to optimize throughput, resulting in up to a 60% improvement in efficiency. Their work emphasizes the need for a systematic approach to draft model design and shows how these improvements can lead to substantial performance gains, such as reducing KV-cache requirements by 37%, enabling larger batch sizes, and outperforming other methods like self-speculative decoding (Zhang et al., 2023).

Liu et al. (2023) proposed continuously training the draft model on the outputs of the target model to improve token acceptance rates, though performing such training during inference remains challenging. Xia et al. (2023) introduced an encoder-decoder-based draft model, providing an alternative to traditional autoregressive architectures. Another line of work focuses on increasing the number of candidate tokens per step, as investigated by Sun et al. (2024b) and Yang et al. (2024), which improves throughput by enhancing the acceptance rate. Additionally, Zhou et al. (2024) explored draft model distillation to create more efficient and compact models, aligning with the goal of reducing computational overhead while maintaining performance. In the context of long-context scenarios, Sun et al. (2024a) and Chen et al. (2024) examined speculative decoding strategies tailored for extended sequences, reinforcing the need for systematic draft model design.

Gu et al. (2025) introduced DART, which integrates autoregressive and diffusion processes within a non-Markovian framework. By eliminating the Markovian assumption that limits traditional diffusion models, DART leverages the full generative trajectory, allowing for more effi-

cient image generation. This approach iteratively denoises image patches using an autoregressive model, enhancing the quality of text-to-image generation. Additionally, DART removes the need for image quantization, significantly improving computational efficiency while maintaining flexibility, ultimately setting a new standard for high-quality, scalable image synthesis.

The LIMINAL model (Gu et al., 2025) provides an analytical framework to assess the fundamental performance limits of Large Language Model (LLM) inference, with a particular focus on the auto-regressive decoding phase. It abstracts hardware and application parameters—such as compute throughput, memory bandwidth, memory capacity, and inter-chip communication latency—enabling the evaluation of system performance across a wide range of existing and projected hardware configurations, including GPUs and TPUs. The model reveals that the performance of LLM inference is primarily constrained by memory bandwidth, synchronization latency, and compute capacity.

B Estimation of Parameter α

To estimate the value of α characterizing a specific pair of draft (M_q) and target (M_p) models, we first estimate the Token Acceptance Rate (TAR) between them. TAR quantifies the probability that a draft token generated by M_q is accepted by M_p during speculative decoding, and thus serves as a key observable reflecting the relationship between the two models.

We measure TAR as a function of the lookahead length γ using the procedure described in Appendix B.1. Once the TAR values are collected, we use them to estimate α by solving an inverse problem: specifically, we fit the observed TARs to the theoretical model given by (12). This fitting involves solving a nonlinear, overdetermined system of nine equations—one for each value of γ —using a least-squares formulation to minimize residuals. We also quantify the uncertainty of the estimated α by constructing confidence intervals, as detailed in Appendix B.2.

B.1 Tokens Accepted Rates

The **Token Acceptance Rate (TAR)** introduced by Yan et al. (2025) serves as a crucial metric in evaluating the performance of speculative decoding algorithms. Defined as the average rate at which tokens generated by the draft model M_q are ac-

cepted by the target model M_p , TAR quantifies the effectiveness of the approximation made by M_q . Empirically, TAR can be achieved by dividing the number of accepted tokens by the number of tokens generated by the draft model M_q during decoding. For a given γ , also called lookahead length representing the maximum number of tokens generated by the draft model, TAR can also be calculated using the formula suggested by Leviathan et al. (2023):

$$\text{TAR}(\gamma) = \frac{1 - \alpha^{\gamma+1}}{1 - \alpha} \quad (12)$$

This equation illustrates how TAR is influenced by the expected acceptance rate α and highlights how well M_q approximates M_p . A higher acceptance rate indicates more efficient sampling, leading to an increased number of tokens produced with each run (Yan et al., 2025).

The draft model M_q samples $x_{1,\dots,\gamma}$ guesses in an autoregressive manner. Specifically, for each guess i (where i ranges from 1 to γ), the probability distribution is computed as follows:

$$q_i(x) = M_q(\text{prefix} + [x_1, \dots, x_{i-1}])$$

Then, a token x_i is sampled from the distribution $q_i(x)$, corresponding to the probability of the next token given the prefix extended by previously sampled guesses. After generating all guesses, the target model M_p computes the probability of each guess by evaluating the extended prefixes (prefix + x_1), (prefix + x_1, x_2), \dots , (prefix + x_1, \dots, x_γ) in parallel.

The number of accepted guesses n is then determined by comparing random samples drawn from a uniform distribution against the ratio of probabilities from the target and draft models:

$$n = \min(\{i - 1 \mid 1 \leq i \leq \gamma, r_i > \frac{p_i(x)}{q_i(x)}\} \cup \{\gamma\})$$

Where $r_i \sim U(0, 1)$ denotes a random sample drawn independently from the uniform distribution for each guess i . This process, repeated across multiple speculative decoding steps, enables empirical measurement of TAR at different lookahead lengths.

After repeating the speculative decoding steps for a fixed γ across multiple trials, the empirical TAR is computed as the mean number of accepted tokens divided by the number of tokens proposed:

$$\text{TAR}_\gamma = \text{mean}(n)$$

This metric provides a practical measure of the average acceptance rate under different lookahead settings, characterizing the efficiency of speculative decoding.

B.2 Calculating confidence intervals for α estimation

Let b_i denote the empirically observed Token Acceptance Rate (TAR) for the specific pair of target and draft models and the corresponding lookahead length γ_i .

- $E(\alpha, \gamma_i)$: Represents the predicted value from the model function for a given parameter α and a specific power γ_i , calculating an expected outcome based on the model, which is theoretical in nature.

The goal of estimating α is to minimize the difference between these two quantities.

Extracting the Residuals and Jacobian After performing the nonlinear least squares fitting, we extract two important components from the optimization result, the residuals and the Jacobian matrix :

1. **Residuals** denoted as $r_i(\alpha)$, represent the differences between the predicted values from our model function $E(\alpha, \gamma_i)$ and the observed TARs b_i . They are defined as:

$$r_i(\alpha) = E(\alpha, \gamma_i) - b_i$$

The collection of all residuals can be expressed in vector form as:

$$\mathbf{r} = \begin{bmatrix} r_1(\alpha) \\ r_2(\alpha) \\ \vdots \\ r_n(\alpha) \end{bmatrix} = \begin{bmatrix} E(\alpha, \gamma_1) - b_1 \\ E(\alpha, \gamma_2) - b_2 \\ \vdots \\ E(\alpha, \gamma_n) - b_n \end{bmatrix}$$

This residual quantifies how far off your model's prediction is from the actual observed TAR. By minimizing these residuals across all data pairs, we can estimate an optimal value for α .

2. **Jacobian Matrix**, denoted as J , contains the first derivatives of the residuals with respect to the parameter α . Mathematically, if we denote

our residuals as $r_i(\alpha)$ for each data pair, then the Jacobian is defined as:

$$J_{i,j} = \frac{\partial r_i(\alpha)}{\partial \alpha}$$

This matrix provides information about how sensitive the residuals are to changes in the parameter α . In other words, it indicates how small changes in α will affect the residuals. The Jacobian is crucial for optimization algorithms because it helps determine the direction and magnitude of updates to the parameter during the fitting process.

Variance of Residuals To estimate the variance of the residuals, we first need to define the total number of observed TARs, denoted as n_{b_i} . The degrees of freedom (dof) are defined as:

$$\text{dof} = n_{b_i} - 1$$

The estimated variance of the residuals is calculated under the assumption that they follow a normal distribution. This is computed using the formula:

$$\sigma_{\text{residual}}^2 = \frac{\sum_{i=1}^{n_{b_i}} r_i^2(\alpha)}{\text{dof}}$$

In this equation, $r_i(\alpha)$ represents the residual for each data pair. By summing the squared residuals and dividing by the degrees of freedom, we obtain an unbiased estimate of the variance of the residuals.

Variance of α , Standard Error, and Confidence Intervals The variance of the estimate for parameter α is given by:

$$\text{Var}(\alpha) = \sigma_{\text{residual}}^2 (J^T J)^{-1}$$

The standard deviation of α is then calculated as:

$$\text{Std}(\alpha) = \sqrt{\text{Var}(\alpha)}$$

To construct a 95% confidence interval for the estimated parameter α , we utilize the standard deviation of the estimate, denoted as $\text{Std}(\alpha)$.

The confidence interval can be expressed as:

$$\text{Lower Bound} = \alpha - z_{0.025} \cdot \text{Std}(\alpha)$$

$$\text{Upper Bound} = \alpha + z_{0.025} \cdot \text{Std}(\alpha)$$

Where:

- $z_{0.025}$ is the critical value from the standard normal distribution corresponding to a 95% confidence level (approximately 1.96).

This methodology allows us to quantify the uncertainty around our estimate of α , providing a range within which we can be 95% confident that the true parameter value lies.

C Optimization of Throughput over γ

We defined γ_{optimal} as the optimal number of tokens that the draft model should generate to maximize throughput. We derived this value by solving the derivative of Equation (3) with respect to γ :

$$\frac{d\mathcal{T}}{d\gamma} = \frac{N - N\alpha^{1+\gamma} + (M + N\gamma)\alpha^{1+\gamma} \log(\alpha)}{2(M + N\gamma)^2(-1 + \alpha)}$$

To find the optimal γ , we check where this derivative equals zero, leading to:

$$\gamma_{\text{opt}} = \frac{-M \log(\alpha) + N W\left(-\frac{\alpha^{(M/N-1)}}{e}\right) + N}{N \log(\alpha)} \quad (13)$$

Substituting (13) into (3) yields the throughput at optimal γ , shown in (4).

Furthermore, by incorporating (5) and (2) into the optimality condition in (13), we derive an explicit expression for γ_{optimal} in terms of the draft and target model parameters:

$$\begin{aligned} \gamma_{\text{opt}} = & \frac{-M \log(Ae^{L(N,D)} + Be^{L(M,D')} + C)}{N \log(Ae^{L(N,D)} + Be^{L(M,D')} + C)} \\ & + \frac{N \cdot W\left(-\frac{(Ae^{L(N,D)} + Be^{L(M,D')} + C)^{(M/N-1)}}{e}\right)}{N \log(Ae^{L(N,D)} + Be^{L(M,D')} + C)} \\ & + \frac{N}{N \log(Ae^{L(N,D)} + Be^{L(M,D')} + C)} \end{aligned} \quad (14)$$

where W denotes the Lambert W function. Since the argument inside $W(x)$ is negative, we specifically use the W_{-1} branch, which provides real solutions in the range $-1/e \leq x < 0$. This selection ensures that γ_{optimal} remains well-defined and avoids complex-valued results. However, since α is always in the range $(0, 1)$ and M is typically much larger than N , the argument of the Lambert W function, $-\frac{\alpha^{(M/N-1)}}{e}$, remains within the valid domain of the W_{-1} branch, ensuring real-valued solutions. This guarantees the applicability of the

derived expression for γ_{optimal} under standard conditions. The model is not applicable when $M < N$.

Note that it is possible to implement a non-integer value of γ by randomizing the choice of the lookahead length between the steps of the speculative decoding procedure. This formula depends on the key architecture hyperparameters M and N of speculative decoding system components, along with α , which captures the alignment between the components.

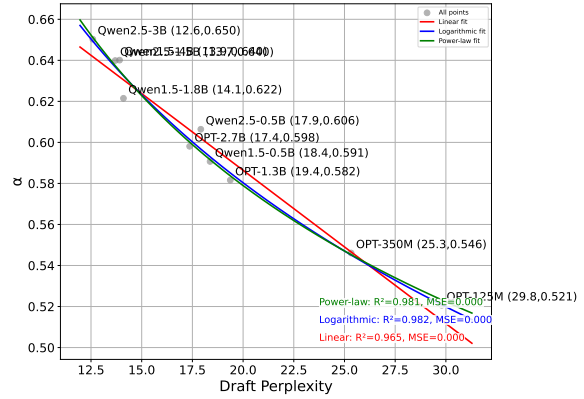
D Regressing α on perplexity of draft models

To analyze the relationship between draft model perplexity (x) and the estimated scaling parameter α , we fitted a set of analytical scaling laws—including power-law, linear, and logarithmic functions—to the data presented in Tables 1 and 2. For each target model, the fits were performed using paired values of draft model perplexity and the corresponding estimated α across multiple draft models. We restrict our analysis to scaling laws with two free parameters, reflecting the limited number of available draft models and, consequently, the small number of data points per target model. The estimated parameters of the fitted scaling laws, together with their margins of error, 95% confidence intervals, mean squared error (MSE), and coefficient of determination (R^2), are summarized in Table 4 for all target models considered. The fitted relationships are illustrated in Figures 3a and 3b.

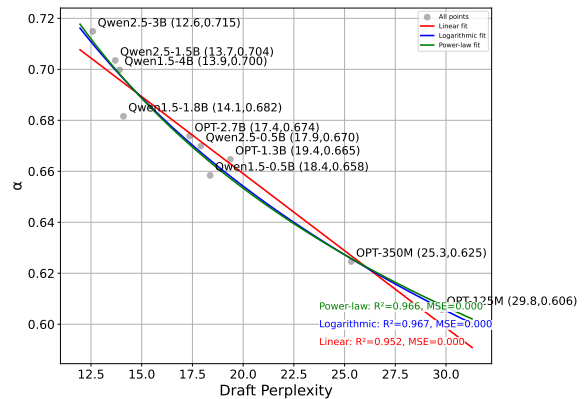
Results. Table 4 and Figure 3 consistently indicate a monotonic relationship between draft model perplexity and the estimated scaling parameter α across all target models and fitted functional forms. In particular, as the perplexity of the draft models decreases, the estimated values of α systematically increase, independent of the specific analytical scaling law employed. This trend is observed for linear, logarithmic, and power-law fits, and is consistent across the full range of target models considered.

E Regressing α on perplexity of target models

Tables 1 and 2 summarize the estimated α values obtained for different combinations of target models and draft models, together with the corresponding perplexities of the target models. Across both tables, α varies only weakly with changes in target model perplexity when the draft model is held



(a) Curves relating the estimated α to the perplexity of the draft models paired with the Qwen1.5-110B target model.



(b) Curves relating the estimated α to the perplexity of the draft models paired with the LLaMA3.1-70B target model.

Figure 3: Curves show estimated α values as a function of draft model perplexity, based on data from Tables 1 and 2. The α values were computed based on the method outlined in Appendix B, which estimates them using accepted token statistics. Function details appear in Table 4.

fixed. In particular, for a given draft model, target models spanning a broad range of perplexity values often yield similar α estimates, with no consistent monotonic trend as a function of target model perplexity.

This behavior contrasts with the strong and systematic dependence of α on draft model perplexity observed in Section D. While higher-quality target models (i.e., those with lower perplexity) sometimes correspond to slightly larger α values, this effect is neither uniform across draft models nor consistent across target model families. In several cases, target models with comparable perplexity produce nearly identical α estimates, despite substantial differences in their absolute perplexity values.

Overall, the results indicate that α is significantly

more sensitive to the perplexity of the draft model than to that of the target model. At the scale of the OPT, Qwen, LLaMa, and Seed target models considered here, we do not observe a robust, quantifiable dependency of α on target model perplexity.

F Latency-based validation of N^* for OPT-13B

In Section 4.3, we analytically derived the optimal draft model size N^* that maximizes the predicted throughput for each target model and draft family by maximizing Equation (9). These predictions are summarized in Table 5. While the analytical formulation captures the dominant computational trade-offs of speculative decoding, it abstracts away system-level effects that can influence real-world inference performance, including kernel launch overheads, memory bandwidth constraints, and model execution overheads. In this subsection, we empirically validate the predicted optimal draft size for the OPT-13B target model by directly measuring speculative decoding latency across all evaluated draft models.

Method. Latency measurements are performed on the HellaSwag dataset. We randomly select 50 prompts and use each prompt independently to measure inference latency. Prompts are tokenized using the target model tokenizer and truncated or padded as needed to ensure compatibility when draft and target models employ different tokenizers.

For each prompt, we measure three latency components: (i) *time-to-first-token (TTFT)*, defined as the time required to generate the first output token under speculative decoding; (ii) *total generation time (TTOT)*, measured for generating a fixed-length continuation of 250 tokens; and (iii) *time-per-output-token (TPOT)*, computed as TTOT divided by the number of generated tokens. Speculative decoding is executed with greedy decoding (no sampling), a maximum generation length of 250 tokens, and batch size one. For draft–target pairs that do not share a tokenizer, both the draft and target tokenizers are explicitly provided during generation to ensure correct token alignment.

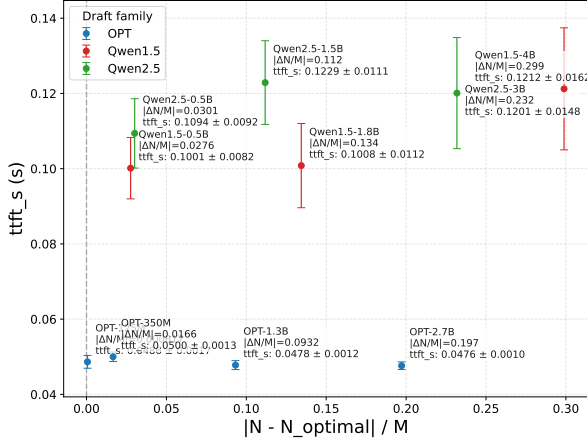
All models are loaded in half precision (float16) and executed on a single A100 GPU. To mitigate one-time initialization effects such as kernel compilation and cache warming, a warm-up phase consisting of a forward pass and a short speculative generation is performed prior to measurement. GPU synchronization is enforced before

and after each timed segment to ensure accurate wall-clock measurements. For each draft model, latency metrics are aggregated across prompts, and we report the mean along with a 95% confidence interval computed using the standard normal approximation. The resulting measurements are summarized in Table 6.

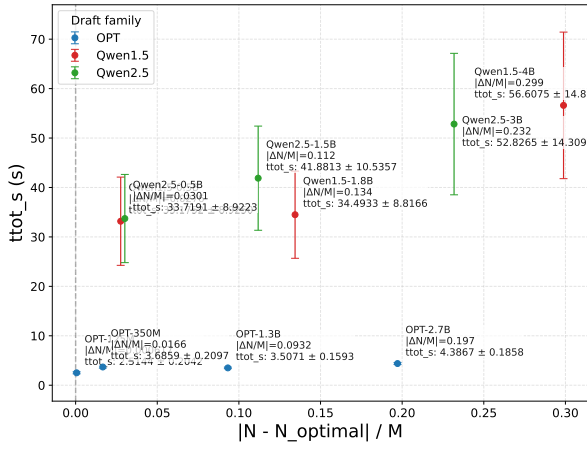
Results and validation. We emphasize that this appendix focuses on OPT-13B as a representative target model, and that absolute latency values may differ across draft families due to architectural and tokenizer differences though the similar trend is expected. Table 6 shows that, across all evaluated draft model families, the minimum observed latency consistently occurs at draft sizes that closely align with the analytically predicted optimal draft size N^* . Draft models whose sizes lie closest to N^* achieve lower TTFT, TTOT, and TPOT compared to both substantially smaller and larger draft models.

This agreement provides empirical support for the throughput-based optimization derived in Section 4.3, demonstrating that maximizing predicted throughput is an effective proxy for minimizing end-to-end inference latency. To quantify deviations from the predicted optimum, we report the normalized distance $|N - N^*|/M$, which measures how far each evaluated draft size deviates from the analytical optimum relative to the target model size. Across all draft families, latency increases monotonically with this normalized distance, indicating that N^* accurately captures the location of the latency minimum even when only a discrete set of draft sizes is available.

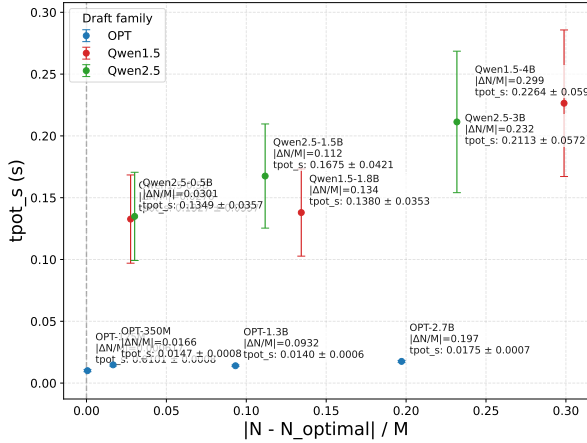
Importantly, Figure 4 shows that this trend holds consistently across heterogeneous draft families, including OPT, Qwen1.5, and Qwen2.5. When latency is plotted as a function of the normalized deviation $|N - N^*|/M$, draft models from all families exhibit their lowest TTFT, TTOT, and TPOT values at or near $|N - N^*|/M = 0$, with latency increasing as draft size deviates further from the analytically predicted optimum. This alignment indicates that the predicted N^* reliably identifies the vicinity of the latency-minimizing draft size for OPT-13B, despite architectural and tokenizer differences across draft families.



(a) Measured time-to-first-token (TTFT) under speculative decoding for OPT-13B as a function of draft model size N .



(b) Measured total generation time (TTOT) for generating 250 tokens under speculative decoding for OPT-13B as a function of draft model size N .



(c) Measured time-per-output-token (TPOT) under speculative decoding for OPT-13B as a function of draft model size N .

Figure 4: Latency metrics (TTFT, TTOT, and TPOT) for the OPT-13B target model plotted as a function of the normalized deviation $|N - N^*|/M$ from the analytically predicted optimal draft size. Each point corresponds to an individual draft model from the OPT, Qwen1.5, or Qwen2.5 families, with error bars indicating 95% confidence intervals across prompts. The vertical dashed line marks the predicted optimum N^* . Across all metrics and draft families, latency increases with distance from N^* , supporting the accuracy of the throughput-based optimal draft size prediction.

As shown in both Figure 4 and Table 6, minor discrepancies between the analytically predicted optimum and the empirically best-performing draft model are observable, particularly for very small or very large draft sizes. These deviations are expected and can be attributed to system-level effects not explicitly captured by Equation (9), including kernel launch overheads, memory bandwidth saturation, and the fixed execution cost of the draft model. Importantly, these effects influence the magnitude of latency but do not shift the overall location of the latency minimum.

Parameter	Estimate	Std. Error	Margin of Error	CI Lower (95%)	CI Upper (95%)
A	-0.0067	0.000607	± 0.001201	-0.007901	-0.005499
B	0.012971	0.001545	± 0.003056	0.009914	0.016027
C	0.642084	0.021228	± 0.042006	0.600078	0.684090
Model Performance					
Mean Squared Error (MSE)			0.001284		
R^2			0.602296		

Table 3: Model coefficients for Equation 5, including standard errors, margins of error, and 95% confidence intervals, along with overall model performance metrics (mean squared error and R^2).

Target Model	Function	Param 1	MoE 1	CI 1	Param 2	MoE 2	CI 2	MSE	R^2
Qwen1.5-14B	Linear	-0.008262	0.001653	[-0.009915, -0.006609]	0.832953	0.031375	[0.801578, 0.864329]	0.000113	0.943203
	Logarithmic	-0.165206	0.026300	[-0.191506, -0.138905]	1.155850	0.075721	[1.080129, 1.231571]	0.000073	0.963273
	Power-law	1.382782	0.158956	[1.223826, 1.541738]	-0.247168	0.040405	[-0.287573, -0.206763]	0.000073	0.963076
Qwen1.5-32B	Linear	-0.007686	0.001206	[-0.008892, -0.006480]	0.804857	0.022886	[0.781971, 0.827743]	0.000060	0.964297
	Logarithmic	-0.153441	0.017053	[-0.170494, -0.136388]	1.104542	0.049097	[1.055444, 1.153639]	0.000031	0.981757
	Power-law	1.302398	0.100870	[1.201528, 1.403268]	-0.235315	0.027208	[-0.262523, -0.208108]	0.000032	0.981142
Qwen1.5-72B	Linear	-0.007030	0.001175	[-0.008205, -0.005854]	0.795392	0.022306	[0.773086, 0.817698]	0.000057	0.959649
	Logarithmic	-0.140489	0.016717	[-0.157205, -0.123772]	1.069918	0.048130	[1.021789, 1.118048]	0.000029	0.979144
	Power-law	1.231728	0.091181	[1.140547, 1.322910]	-0.214429	0.025980	[-0.240409, -0.188449]	0.000029	0.979229
Qwen1.5-110B	Linear	-0.007472	0.001156	[-0.008627, -0.006316]	0.735836	0.021937	[0.713899, 0.757774]	0.000055	0.965252
	Logarithmic	-0.149112	0.016424	[-0.165536, -0.132688]	1.027021	0.047286	[0.979735, 1.074306]	0.000028	0.982076
	Power-law	1.238509	0.103323	[1.135185, 1.341832]	-0.253840	0.029332	[-0.283173, -0.224508]	0.000030	0.981240
Qwen2.5-14B	Linear	-0.006945	0.001348	[-0.008293, -0.005597]	0.798363	0.025582	[0.772782, 0.823945]	0.000075	0.946381
	Logarithmic	-0.138591	0.022254	[-0.160845, -0.116337]	1.068989	0.064071	[1.004917, 1.133060]	0.000052	0.962659
	Power-law	1.224068	0.120964	[1.103104, 1.345032]	-0.209879	0.034674	[-0.244554, -0.175205]	0.000053	0.962049
Qwen2.5-32B	Linear	-0.008567	0.001877	[-0.010444, -0.006690]	0.817586	0.035625	[0.781960, 0.853211]	0.000145	0.932654
	Logarithmic	-0.171822	0.029227	[-0.201049, -0.142594]	1.153888	0.084149	[1.069739, 1.238037]	0.000090	0.958285
	Power-law	1.414605	0.183098	[1.231507, 1.597702]	-0.266090	0.045535	[-0.311625, -0.220556]	0.000087	0.959765
Qwen2.5-72B	Linear	-0.008433	0.001991	[-0.010425, -0.006442]	0.808611	0.037793	[0.770817, 0.846404]	0.000164	0.922622
	Logarithmic	-0.169348	0.031547	[-0.200895, -0.137801]	1.140266	0.090828	[1.049438, 1.231094]	0.000105	0.950383
	Power-law	1.396431	0.196270	[1.200161, 1.592701]	-0.265035	0.049443	[-0.314478, -0.215592]	0.000100	0.952501
LLaMa3-70B	Linear	-0.008005	0.001788	[-0.009793, -0.006218]	0.831441	0.033928	[0.797514, 0.865369]	0.000132	0.930224
	Logarithmic	-0.160434	0.028584	[-0.189018, -0.131850]	1.145350	0.082296	[1.063054, 1.227646]	0.000086	0.954422
	Power-law	1.357741	0.165924	[1.191817, 1.523664]	-0.239126	0.042938	[-0.282064, -0.196187]	0.000084	0.955649
LLaMa3.1-70B	Linear	-0.006045	0.001108	[-0.007153, -0.004937]	0.779966	0.021028	[0.758937, 0.800994]	0.000051	0.951894
	Logarithmic	-0.120517	0.018271	[-0.138788, -0.102246]	1.015201	0.052604	[0.962596, 1.067805]	0.000035	0.966577
	Power-law	1.129190	0.091637	[1.037553, 1.220828]	-0.182634	0.028439	[-0.211073, -0.154196]	0.000036	0.965962
OPT-13B	Linear	-0.004219	0.001611	[-0.005830, -0.002608]	0.732211	0.030576	[0.701635, 0.762787]	0.000107	0.820131
	Logarithmic	-0.079686	0.037777	[-0.117463, -0.041910]	0.883694	0.108763	[0.774931, 0.992457]	0.000150	0.747328
	Power-law	0.926916	0.159383	[0.767533, 1.086300]	-0.121164	0.060080	[-0.181243, -0.061084]	0.000157	0.737010
OPT-30B	Linear	-0.004025	0.000950	[-0.004975, -0.003075]	0.801596	0.018032	[0.783564, 0.819628]	0.000037	0.922662
	Logarithmic	-0.077500	0.024004	[-0.101504, -0.053496]	0.950355	0.069110	[0.881244, 1.019465]	0.000061	0.873879
	Power-law	0.987912	0.097590	[0.890322, 1.085502]	-0.106544	0.034491	[-0.141035, -0.072053]	0.000064	0.866974
OPT-66B	Linear	-0.004553	0.000804	[-0.005357, -0.003749]	0.850306	0.015264	[0.835042, 0.865571]	0.000027	0.955174
	Logarithmic	-0.088115	0.022067	[-0.110182, -0.066048]	1.019858	0.063533	[0.956325, 1.083391]	0.000051	0.913782
	Power-law	1.066712	0.093086	[0.973626, 1.159797]	-0.115104	0.030481	[-0.145586, -0.084623]	0.000055	0.906985
Seed-OSS-36B	Linear	-0.005858	0.001169	[-0.007027, -0.004689]	0.704290	0.022195	[0.682095, 0.726486]	0.000056	0.943444
	Logarithmic	-0.117008	0.019092	[-0.136100, -0.097916]	0.932871	0.054969	[0.877903, 0.987840]	0.000038	0.961488
	Power-law	1.056024	0.099654	[0.956369, 1.155678]	-0.199176	0.033095	[-0.232271, -0.166081]	0.000038	0.961522

Table 4: Complete regression results for linear, logarithmic, and power-law fits of α as a function of draft model perplexity, including parameter estimates, margins of error (MoE), 95% confidence intervals (CI), mean squared error (MSE), and coefficient of determination (R^2).

Target Model	M (target size)	D' (training target size)	Draft Family	D (training draft size)	N^* (Optimal N)	$\mathcal{T}(N^*)$
Qwen1.5-14B	14167290880	3T	OPT	180B	124039820.3	8.947e-11
			Qwen1.5	2.4T	115390938.2	9.165e-11
			Qwen2.5	18T	112685392.4	9.235e-11
Qwen1.5-32B	32512218112	3T	OPT	180B	198605884.7	4.061e-11
			Qwen1.5	2.4T	184494249.2	4.154e-11
			Qwen2.5	18T	180081907.1	4.183e-11
Qwen1.5-72B	72287920128	3T	OPT	180B	317168451.4	1.883e-11
			Qwen1.5	2.4T	294269636.4	1.924e-11
			Qwen2.5	18T	287112608.1	1.936e-11
Qwen1.5-110B	111209914368	3T	OPT	180B	410570760.1	1.241e-11
			Qwen1.5	2.4T	380698767.3	1.267e-11
			Qwen2.5	18T	371364065.7	1.275e-11
Qwen2.5-14B	14770033664	18T	OPT	180B	126997571.6	8.556e-11
			Qwen1.5	2.4T	118129957.5	8.762e-11
			Qwen2.5	18T	115356193.9	8.829e-11
Qwen2.5-32B	32763876352	18T	OPT	180B	199582637.5	4.005e-11
			Qwen1.5	2.4T	185393085.4	4.095e-11
			Qwen2.5	18T	180956639.7	4.124e-11
Qwen2.5-72B	72706203648	18T	OPT	180B	318409631.5	1.861e-11
			Qwen1.5	2.4T	295409960.3	1.900e-11
			Qwen2.5	18T	288221790.3	1.912e-11
LLaMa3-70B	70553706496	15T	OPT	180B	312760391.8	1.916e-11
			Qwen1.5	2.4T	290182058.1	1.957e-11
			Qwen2.5	1.4T	283125440.3	1.970e-11
LLaMa3.1-70B	70553706496	15T	OPT	180B	312760391.8	1.916e-11
			Qwen1.5	2.4T	290182058.1	1.957e-11
			Qwen2.5	18T	283125440.3	1.970e-11
OPT-13B	12853473280	180B	OPT	180B	117313808.6	1.009e-10
			Qwen1.5	2.4T	109171489.6	1.034e-10
			Qwen2.5	18T	106623620.8	1.043e-10
OPT-30B	29974540288	180B	OPT	180B	189210723.1	4.510e-11
			Qwen1.5	2.4T	175814080.3	4.616e-11
			Qwen2.5	18T	171624238.6	4.650e-11
OPT-66B	65693122560	180B	OPT	180B	299138626.9	2.122e-11
			Qwen1.5	2.4T	277613865.6	2.169e-11
			Qwen2.5	18T	270884739.1	2.184e-11
Seed-OSS-36B	36151104512	12T	OPT	180B	211245817.4	3.649e-11
			Qwen1.5	2.4T	196196967	3.730e-11
			Qwen2.5	18T	191492038.2	3.757e-11

Table 5: Let optimal draft model characteristics for each target model. For each target, we report the model size M , training dataset size D , and the optimal draft model size N that maximizes decoding throughput. The last column reports the achieved throughput in tokens per FLOP for each target model in the measured optimal draft model. This table provides the empirical foundation for our scaling law analysis, illustrating how optimal draft configurations vary with model scale and data.

Draft Model	Draft Family	N^* (Optimal N)	$ N - N^* /M$	TTFT (s)	TTOT (s)	TPOT (s)
OPT-125M	OPT	117M	0.000617	0.04864 ± 0.0017	2.514 ± 0.2042	0.01006 ± 0.00082
OPT-350M	OPT	117M	0.01664	0.050003 ± 0.00126	3.686 ± 0.20972	0.01474 ± 0.00084
OPT-1.3B	OPT	117M	0.09324	0.04779 ± 0.00118	3.507 ± 0.1593	0.01403 ± 0.00064
OPT-2.7B	OPT	117M	0.1972	0.04762 ± 0.00101	4.387 ± 0.1858	0.01755 ± 0.00074
Qwen1.5-0.5B	Qwen1.5	109M	0.0276	0.1001 ± 0.00816	33.18 ± 8.925	0.1327 ± 0.0357
Qwen1.5-1.8B	Qwen1.5	109M	0.1344	0.1008 ± 0.01120	34.49 ± 8.817	0.138 ± 0.03527
Qwen1.5-4B	Qwen1.5	109M	0.2988	0.1212 ± 0.01622	56.61 ± 14.82	0.2264 ± 0.05929
Qwen2.5-0.5B	Qwen2.5	107M	0.03014	0.1094 ± 0.00922	33.72 ± 8.922	0.1349 ± 0.03569
Qwen2.5-1.5B	Qwen2.5	107M	0.1118	0.1229 ± 0.01112	41.88 ± 10.54	0.1675 ± 0.04214
Qwen2.5-3B	Qwen2.5	107M	0.2318	0.1201 ± 0.01477	52.83 ± 14.31	0.2113 ± 0.05724

Table 6: Latency-based validation of the analytically predicted optimal draft size N^* for speculative decoding with an OPT-13B target model. For each evaluated draft model, we report the predicted optimum N^* , the normalized distance $|N - N^*|/M$, and empirical latency measurements obtained from speculative decoding on 50 HellaSwag prompts. Latency metrics include time-to-first-token (TTFT), total generation time (TTOT), and time per output token (TPOT), reported as mean \pm margin of error corresponding to 95% confidence intervals.

Parameter	Range	Number of Grid Points	Description
N	10^8 to 10^{10}	10000	Initial draft model size
M	13×10^9 to 110×10^9	8	Target model size
D	10^{12} to 10^{13}	6	Number of tokens used in draft model training
D'	10^{12} to 10^{13}	6	Number of training tokens used in target model training

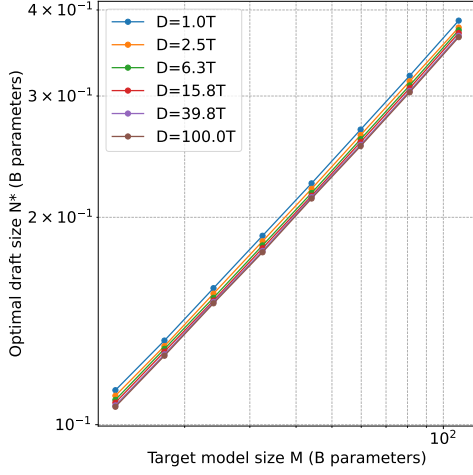
Table 7: Ranges for N , D , and M used in the analysis.

Parameter	Estimate	MoE (95%)	95% CI (lower)	95% CI (upper)
μ	4.89×10^{-3}	7.64×10^{-4}	4.12×10^{-3}	5.65×10^{-3}
M_0	7.23×10^7	1.46×10^6	7.09×10^7	7.38×10^7
γ	-6.07×10^{-5}	1.79×10^{-5}	-7.86×10^{-5}	-4.28×10^{-5}
γ'	1.16×10^{-6}	1.78×10^{-5}	-1.67×10^{-5}	1.90×10^{-5}
R^2	0.978			
Adj. R^2	0.978			
Draft-size search grid	$ N = 10000$ (log-spaced; evaluated only for $N < 10B$)			
Number of Grid Points	$ M = 8, D = 6, D' = 6$			
Observations	288			
Regression type	OLS with HC3 robust standard errors			

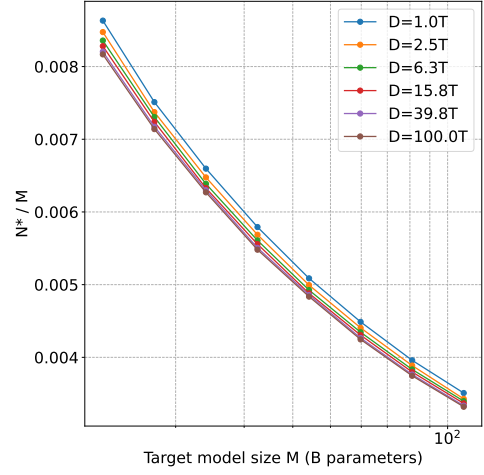
Table 8: Scaling-law regression results for the throughput-optimal draft size. The model $N/M = \mu + M_0/M + \gamma \log D + \gamma' \log D'$ is fit using ordinary least squares with heteroskedasticity-robust (HC3) standard errors. Margins of error (MoE) correspond to half-widths of the reported 95% confidence intervals.

Parameter	Estimate	MoE (95%)	95% CI (lower)	95% CI (upper)
μ	2.71×10^{-3}	4.38×10^{-5}	2.67×10^{-3}	2.75×10^{-3}
M_0	8.71×10^7	2.18×10^6	8.50×10^7	8.93×10^7
R^2	0.9865			
Observations	288			
Number of Grid Points	$ M = 8, D = 6, D' = 6$			
Regression type	OLS with HC3 robust standard errors			

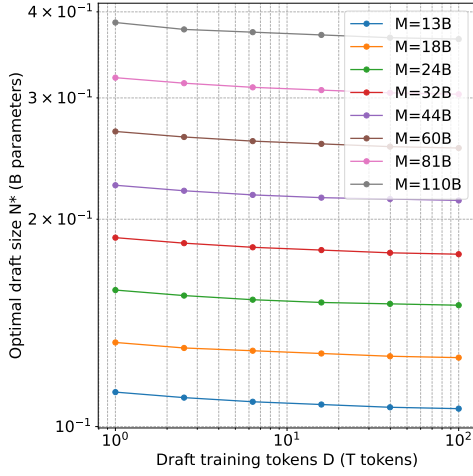
Table 9: Pooled regression results for the leading-order scaling law $N = \mu M + M_0$. The regression is performed over all (M, D, D') configurations, treating dataset-induced variation as part of the residual. Margins of error (MoE) correspond to half-widths of the reported 95% confidence intervals.



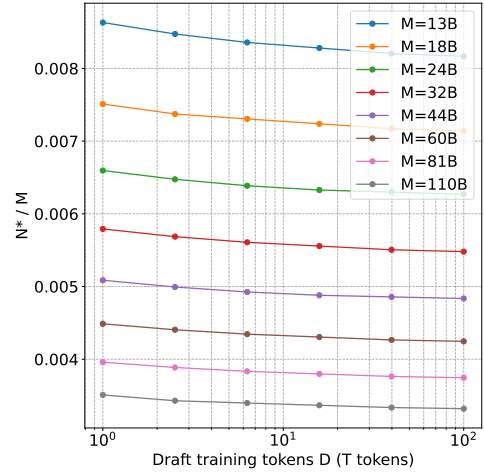
(a) Optimal draft size N^* as a function of target model size M , shown for multiple draft training dataset sizes D while fixing the target training dataset size D' .



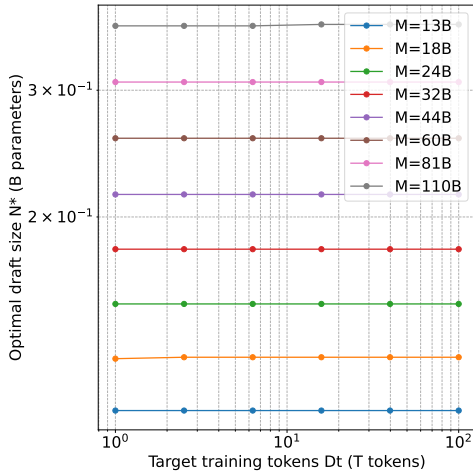
(b) Normalized optimal draft size N^*/M as a function of M , corresponding to Fig. 5a.



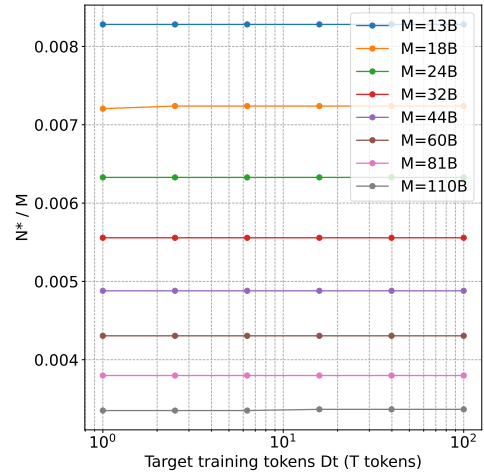
(c) Optimal draft size N^* as a function of draft training dataset size D , shown for multiple target model sizes M while fixing D' .



(d) Normalized optimal draft size N^*/M as a function of D , corresponding to Fig. 5c.



(e) Optimal draft size N^* as a function of the target training dataset size D' , shown for multiple target model sizes M while fixing the draft training dataset size D .



(f) Normalized optimal draft size N^*/M as a function of D' , corresponding to Fig. 5e.

Figure 5: Numerical characterization of the throughput-optimal draft model size N^* as a function of the target model size M , the draft training dataset size D , and the target training dataset size D' . Each row presents the raw dependence of N^* (left) alongside the corresponding normalized view N^*/M (right). The results show that the dominant scaling of the optimal draft size is approximately linear in the target model size, while the effects of the training dataset sizes act as weaker, second-order corrections.